

Combining Q2MM modeling and kinetic studies for refinement of the osmium-catalyzed asymmetric dihydroxylation (AD) mnemonic

Peter Fristrup, Gitte Holm Jensen, Marie Louise Nygaard Andersen,
David Tanner *, Per-Ola Norrby *

Department of Chemistry, Technical University of Denmark, Building 201 Kemitorvet, DK- 2800 Kgs. Lyngby, Denmark

Received 29 September 2005; received in revised form 7 November 2005; accepted 7 November 2005

Available online 13 December 2005

Abstract

The interactions between the substrate and the ligand in the Sharpless AD reaction have been examined in detail, using a combination of substrate competition experiments and molecular modeling of transition states. There is a good agreement between computational and experimental results, in particular for the stereoselectivity of the reaction. The influence of each moiety in the second-generation ligand (DHQD)₂PHAL on the rate and selectivity of the reaction has been elucidated in detail.

© 2005 Elsevier B.V. All rights reserved.

Keywords: Osmium; Asymmetric synthesis; Dihydroxylation; Molecular modeling; Kinetics

1. Introduction

In 1980, Hentges and Sharpless published a seminal paper describing asymmetric induction in the reaction of osmium tetroxide with alkenes [1]. The process required a stoichiometric amount of osmium, and relied on the “pseudoeantiomeric” ligands dihydroquinine acetate and dihydroquinidine acetate, respectively, for induction of chirality in the diol products (25–90% ee). This relatively humble beginning was followed by a major breakthrough in 1988, when the reaction was made catalytic by Sharpless and coworkers by use of *N*-methyl-morpholine-*N*-oxide as a reoxidant [2]. Rapid development of the process then followed, resulting in new ligands for acceleration of the reaction and experimental protocols which are operationally simple, provide excellent chemical yields and enantioselectivities for a wide range of 1,2-diols at low catalyst loadings, and equally easy access to both enantiomers of a given chiral diol [3]. The Sharpless osmium-catalyzed asymmetric dihydroxylation (AD) reaction thus serves as

a benchmark for research in the burgeoning field of catalytic asymmetric synthesis, and has found extensive use in target-oriented synthesis [4]. An empirical mnemonic device was introduced (Fig. 1, left) [5] and later refined (Fig. 1, middle) [6] for prediction of absolute stereochemistry, and a number of mechanistic investigations have appeared, including kinetic [6,7], computational [8–11], and isotope effect [12] studies. We recently published an updated version of the AD mnemonic (Fig. 1, right) [13] and in the current paper we describe how a combination of Q2MM modeling [14] and kinetic measurements can be used to further refine our understanding of the factors underlying the selectivity in the AD reaction.

The revised mnemonic by Sharpless and coworkers (Fig. 1, middle) [6], based upon kinetic [6] and modeling [9] studies, importantly identified that an area of the catalytic complex could provide stabilization for the substrate, and thus rationalized the phenomenon of ligand accelerated catalysis (LAC) [15] that had been observed in the AD reaction. Our work on substrate selectivities extended this concept and suggested that two separate areas provide independent stabilization in two different regions of the ligand [13]. The first of these is identical to the one

* Corresponding author. Tel.: +45 4525 2123; fax: +45 4593 3968.
E-mail address: pon@kemi.dtu.dk (P.-O. Norrby).

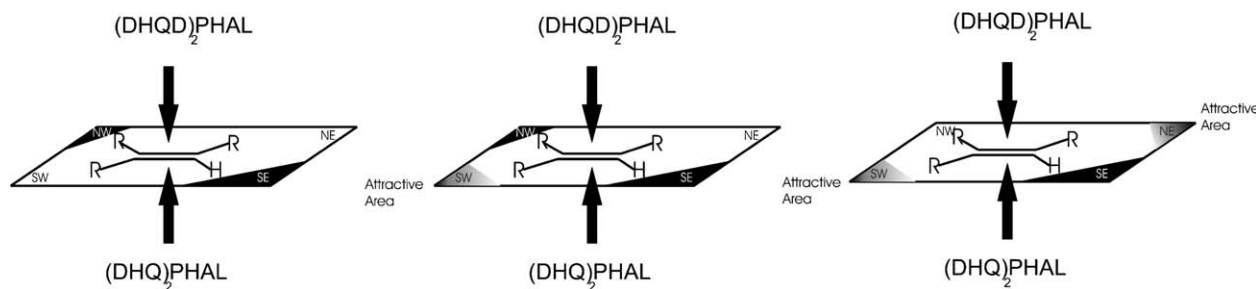


Fig. 1. Left: The original mnemonic device proposed by Sharpless and coworkers [5]. Middle: The revised version of the mnemonic device proposed by Sharpless and coworkers [6]. Right: The modified mnemonic device recently proposed by Norrby and coworkers [13].

identified by Sharpless and coworkers, caused by interactions between alkene substituents and the aromatic linker of the AD-ligand [9], whereas the second corresponds to the interactions with the quinoline moieties first postulated by Corey et al. [16] (Fig. 2).

For simple systems, it has been shown that fair predictions of experimental selectivity can be obtained by manual selection of a few transition state structures followed by computational optimization to the transition states and comparison of the energies thus calculated [10]. However, to obtain quantitative predictions for flexible systems, it is necessary to sample the space of all possible transition states, either by regular conformational searching or molecular dynamics [11,13], followed by Boltzmann population analysis. The number of conformations to be sampled calls for a relatively simple and fast computational method. At the present level of computer technol-

ogy, this requires the use of molecular mechanics force fields, either in conjunction with a DFT representation for the reaction center (QM/MM), or by employing force fields designed to represent the transition states accurately. In the current work, we have chosen the latter approach, utilizing TS force fields based on our own Q2MM methodology [14], which has previously been shown to give highly accurate results for the AD reaction [11].

2. Experimental results

Recently, we have published a limited study of selectivity and reactivity of two groups of tri-substituted alkenes [13]. This study led to the development of a modified mnemonic device, which is able to predict the absolute configuration of the diol product (Fig. 1, right).

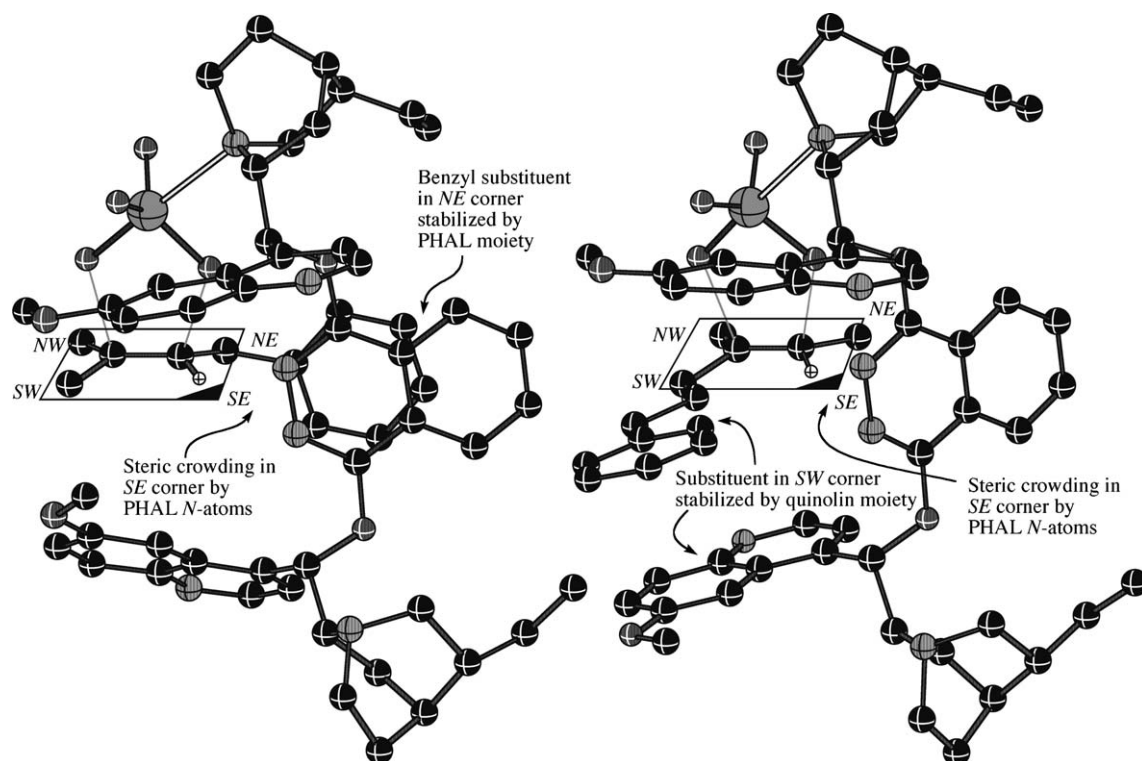


Fig. 2. Illustration of the two attractive pockets described by Sharpless (left) and Corey (right). The TS structures of **2a** (left) and **4b** (right) have been oriented in accordance with the Sharpless mnemonic device.

Here we wish to expand the study to include two new groups of tri-substituted alkenes, as well as a wider set of reaction conditions. All alkenes included in the current study are shown in Fig. 3.

The alkenes from the previous study have been included in the discussion to present a complete picture of the selectivity-determining interactions in the AD reaction. The tri-substituted alkenes are ideal probes in this particular reaction, since the large steric crowding in the so-called SE corner of the mnemonic device (Fig. 1) only allows the orientation where the vinylic hydrogen of the substrate is pointing towards the SE corner. Alkenes denoted **a** will

thus orient the large substituent into the NE corner, where it can interact favorably with the PHAL linker, the Sharpless pocket [6,9]. Similarly, the large substituents of the **b** alkenes go into the SW corner where they can be stabilized by the ligand quinolines, the orientation suggested by Corey and Noe [16]. Finally, the substituents of the **c** alkenes must go into the NW corner, where the Sharpless mnemonic predicted a minor steric interference [5,6], whereas our modified mnemonic simply predicts an absence of stabilizing interactions [13]. With the longest chains (alkenes **3** and **4**), we expect that the flexibility of the substituent will allow it to orient itself into any proximal stabilizing area of the ligand, and thus the difference between substituents should be lower than for the more rigid alkenes **1** and **2**.

The relative rates of reactivity within each class of alkenes are determined by pair-wise competition experiments, where the rate of disappearance of the alkenes is followed by GC, as described previously [13]. Since the reaction is first order in each alkene, and of equal order for all other reagents, the relative rate of any two alkenes in competition is trivially obtained as the slope in a plot of $\ln([\text{alkene}]_0/[\text{alkene}])$ for one alkene against the other. The plots obtained for all four groups of alkenes reacted with stoichiometric OsO_4 in toluene are shown in Figs. 4–7. Within each group of isomeric alkenes, one was selected as reference compound either since it had a reactivity in between that of the other two alkenes or simply due to ease of separation (GC).

For the first two groups of alkenes the differences in reactivity within the group was rather large. This called for the use of the alkene with an intermediate reactivity

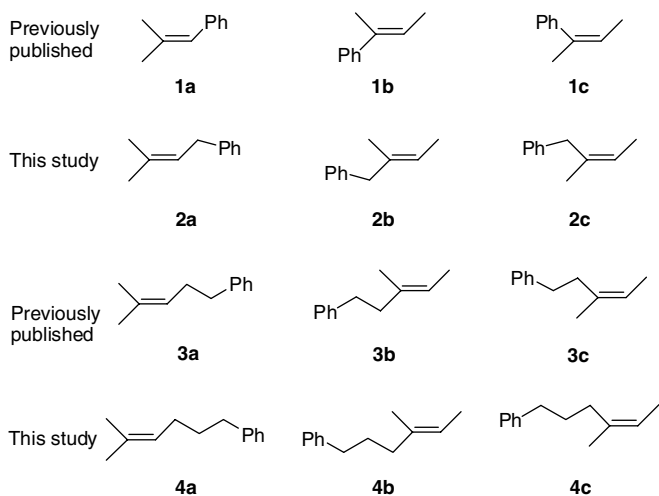


Fig. 3. The four sets of alkenes used to investigate the selectivity-controlling features in the AD-reaction.

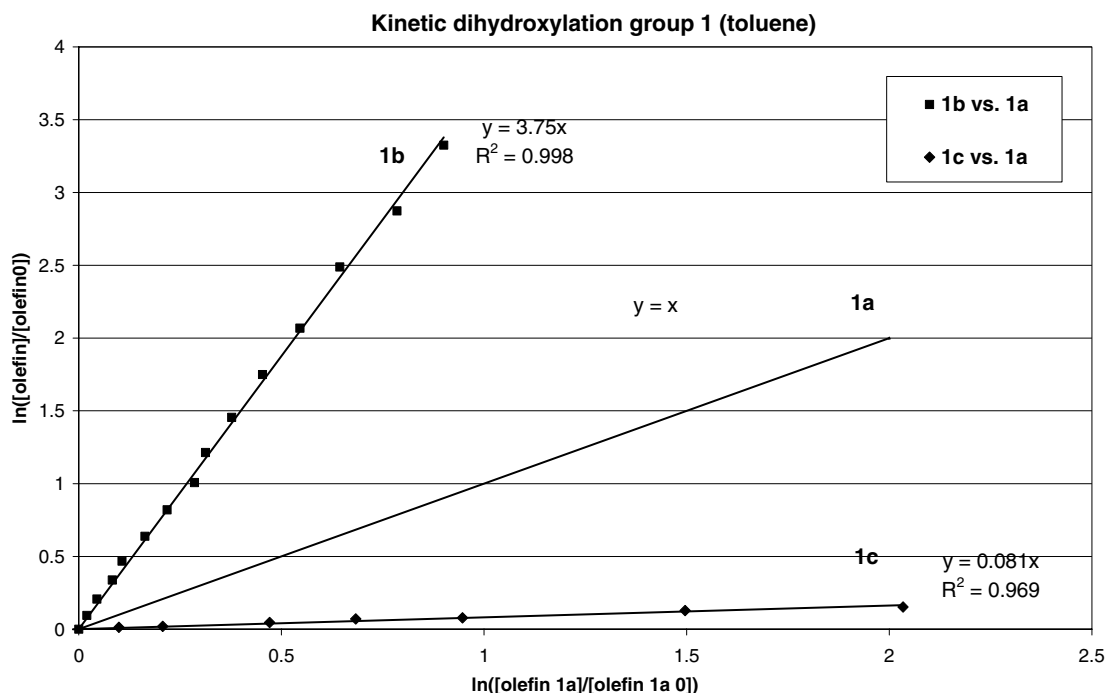


Fig. 4. Relative rates of reaction within group 1. **1b** and **1c** were both measured against **1a** and for this reason **1a** has the relative rate 1 ($y = x$).

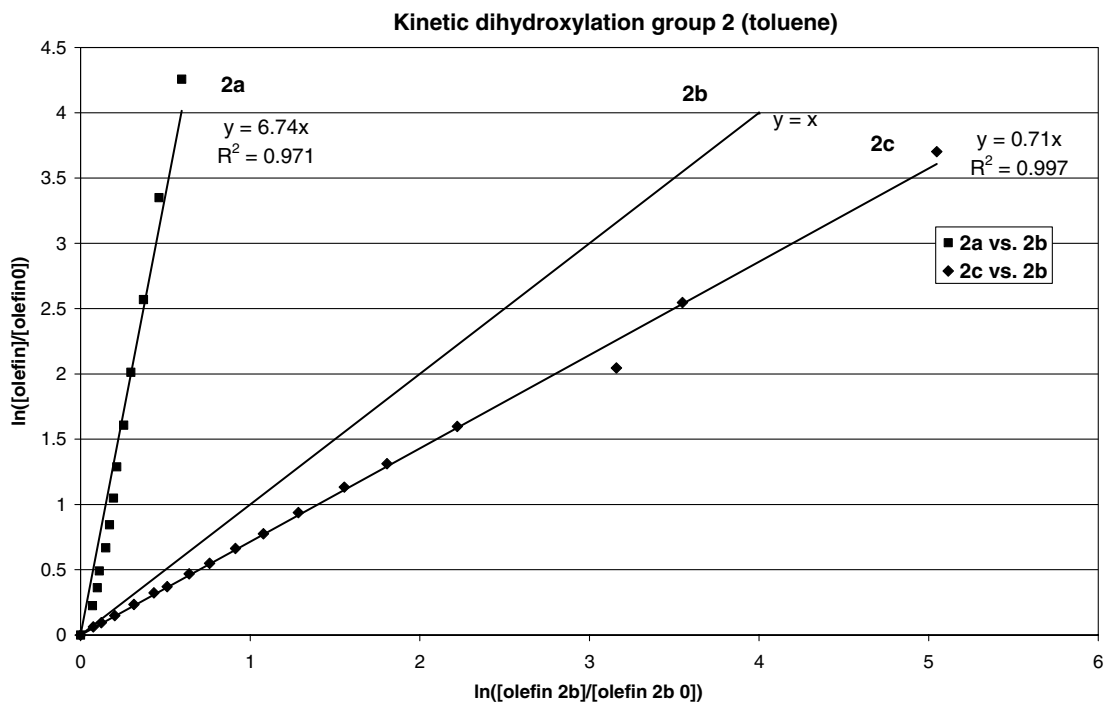


Fig. 5. The relative rates of reaction within group 2.

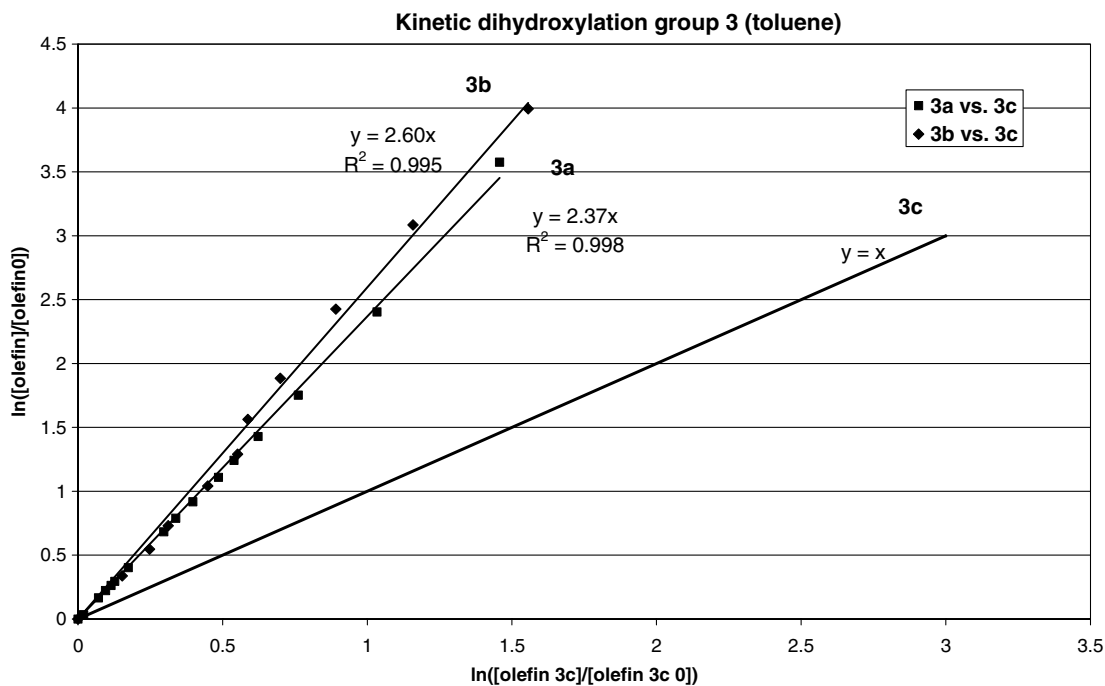


Fig. 6. The results of the kinetic dihydroxylation with the group 3 alkenes.

to be used a reference compound (i.e., alkene **1b** in group **1** and alkene **2b** in group **2**). Within groups **3** and **4** the alkenes could not all be separated on GC, which made it necessary to use the alkenes **3c** and **4a** as reference compounds. Within these groups the differences in reactivity were rather small, so the accuracy in the determination

of relative reactivity was unaffected by the choice of reference compound.

Compound **1b** is clearly the fastest reacting alkene, documenting the importance of the stabilizing interactions in the SW corner of the Sharpless mnemonic (Fig. 1). Substrate **1a** is the second fastest reacting alkene,

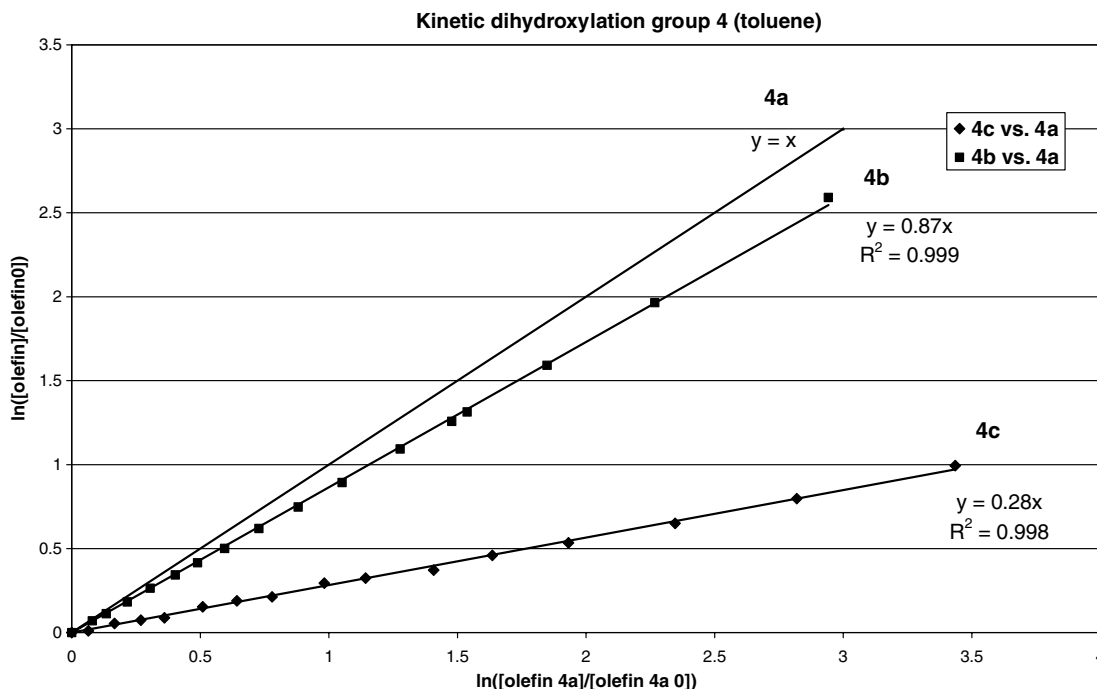


Fig. 7. The results of the kinetic dihydroxylation of the alkenes **4**.

approximately four times slower than **1b**. The fact that it is more than 10 times faster than the slowest reacting alkene (**1c**) shows the NE corner also interacts favorably with the phenyl group. The slowest reacting alkene (**1c**) points the phenyl group towards the NW corner of the Sharpless mnemonic, which does not afford stabilization. The results from group **1** reveal a difference in reaction rate of more than a factor of 40 between the slowest and the fastest alkene. The large difference can be attributed to the fact that the phenyl group is connected directly to the double bond, and the conjugation does not allow the phenyl group to rotate freely to relieve strain or steric repulsion inside the pocket created by the ligand. The results from group **1** are in accordance with the original Sharpless mnemonic [6], which singles out the SW corner as especially attractive towards aromatic groups.

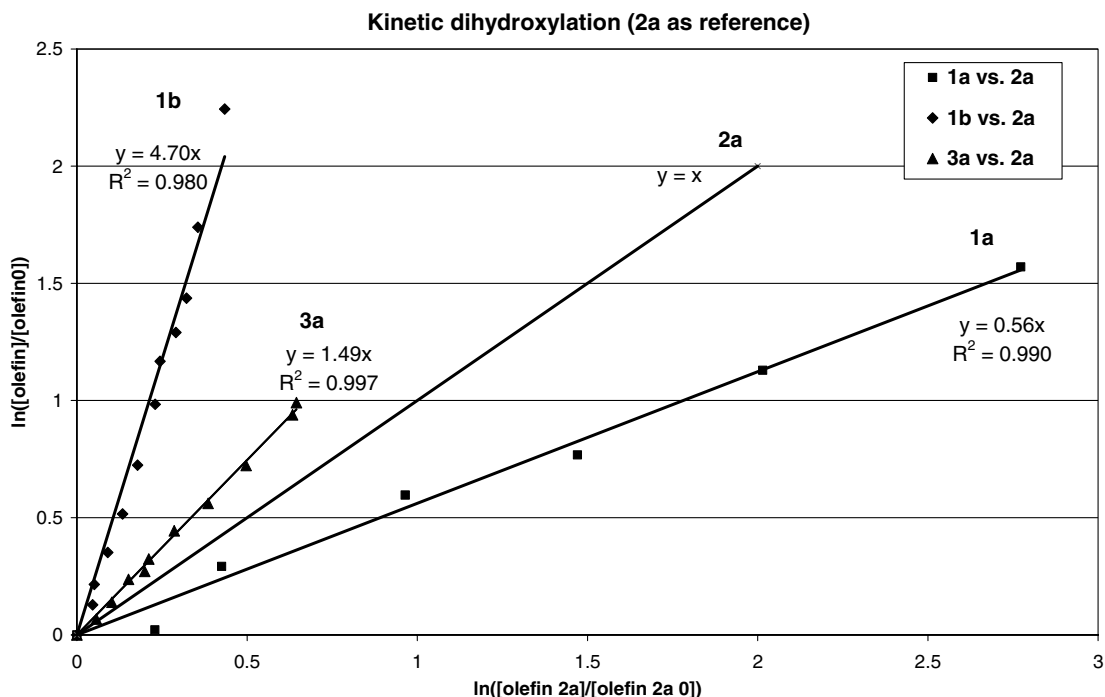
The group **2** alkenes were investigated in a similar manner and the results are shown in Fig. 5. Within this group **2a** is by far the fastest reacting alkene. Clearly this means that the NE corner is far better in stabilizing a benzyl group than any other corner. Alkene **2b** reacts about 40% faster than **2c**, which shows that the SW corner is only marginally better in stabilizing a benzyl group than the NW corner. These results are in sharp contrast to the predictions from the Sharpless revised mnemonic (Fig. 1, middle) which predicts the SW corner to be more favorable than NE. Our own revised mnemonic (Fig. 1, right) does not attempt to differentiate between the SW and NE corners, and the results from alkenes **1** and **2** clearly show that no such differentiation is possible with such a simple device.

The results for the group **3** alkenes are shown in Fig. 6. In this case two parts of the osmium–ligand complex, cor-

responding to the NE and SW corners of the mnemonic device, are equally good in stabilizing the aromatic part of the alkene. Again, this is in contrast to the revised mnemonic device suggested by Sharpless, but in good agreement with the mnemonic device suggested by us previously (Fig. 1, right). The difference in reactivity is much smaller for this substrate group than for the previous group. This can be attributed to the fact that the phenyl groups in alkenes **3** and **4** are connected to the double bond with a flexible tether, allowing it to reach through space towards any stabilizing interactions available, with less dependence on the position of the origin of the tether.

The results for the kinetic dihydroxylation of group **4** are shown in Fig. 7. The same explanations as the ones advanced for group **3** can also be applied here. Substrates **4a** and **4b** show very similar reactivity. The slowest reacting alkene is **4c**, which has the large group in the NW corner. This alkene can obtain stabilizing interactions only by “wrapping” around to the other areas of the ligand.

Having established the relative rates of reactivity for the one-phase system in toluene, we turned our attention to the more synthetically useful two-phase *t*-BuOH:H₂O solvent system. Our initial results using alkenes from group **1** were unsuccessful due to too large differences in reactivity between the substrates. When the difference in reactivity approaches a factor of 10 the changes in the concentration of the slowest reacting alkene become very small, thus leading to large uncertainties in the determination. Instead, we chose to select competing pairs from the entire set of 12 alkenes, based solely upon relative reactivity. Using alkene **2a** as reference compound the relative reactivities of **1a**, **1b** and **3a** could be established (Fig. 8).

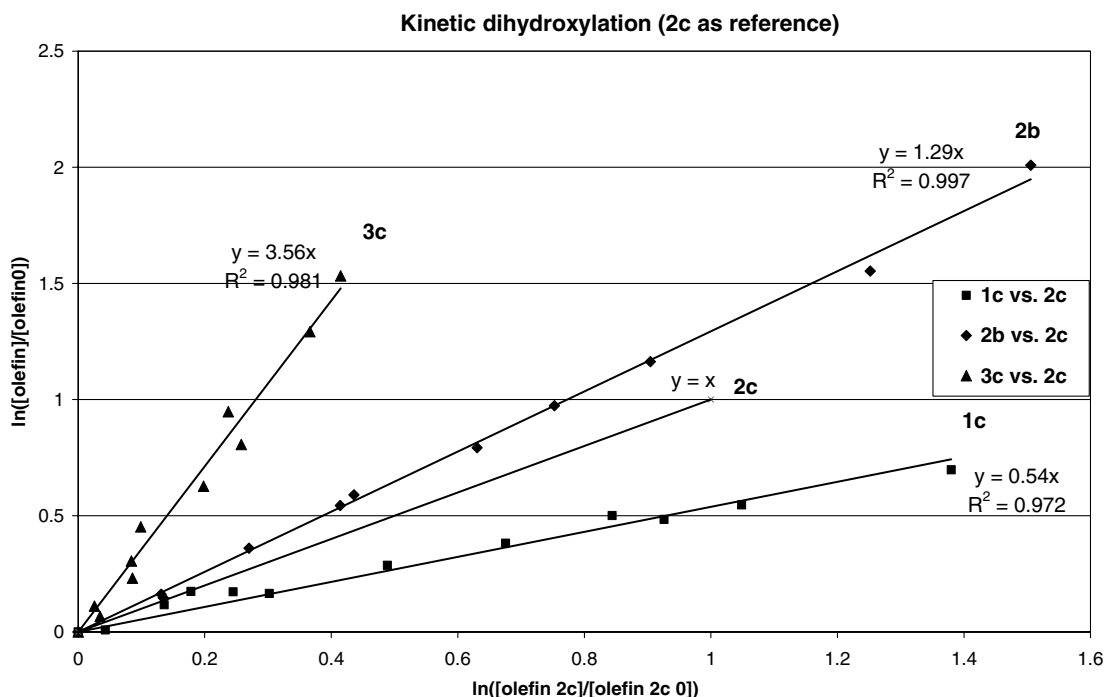


The reactivity of the substantially slower-reacting **c** alkenes from groups **1–3** was determined relative to alkene **2c**, and it was also possible to determine the relative reactivity of alkene **2b** in the same group (Fig. 9).

For the group **3** alkenes it was possible to determine the relative reactivity of all three alkenes within the group, and in addition alkene **4b** could also be related to **3b** (Fig. 10).

The remaining determinations of relative reactivities have been collected in Fig. 11.

The results of the kinetic dihydroxylation are summarized in Fig. 12. A dotted arrow indicates the difference in reactivity was too large to be determined. A full line arrow indicates the difference in reactivity could be determined. The reactivity of each alkene compared



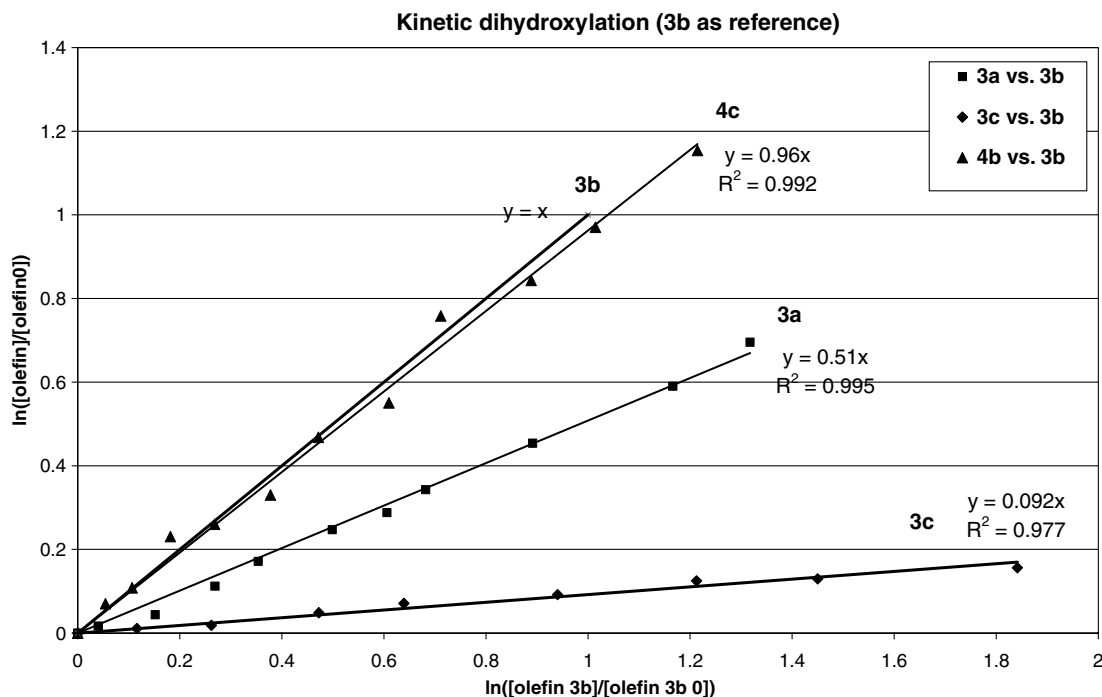


Fig. 10. Kinetic plots for alkenes **3a**, **3c** and **4c**, which were all determined relative to alkene **3b**.

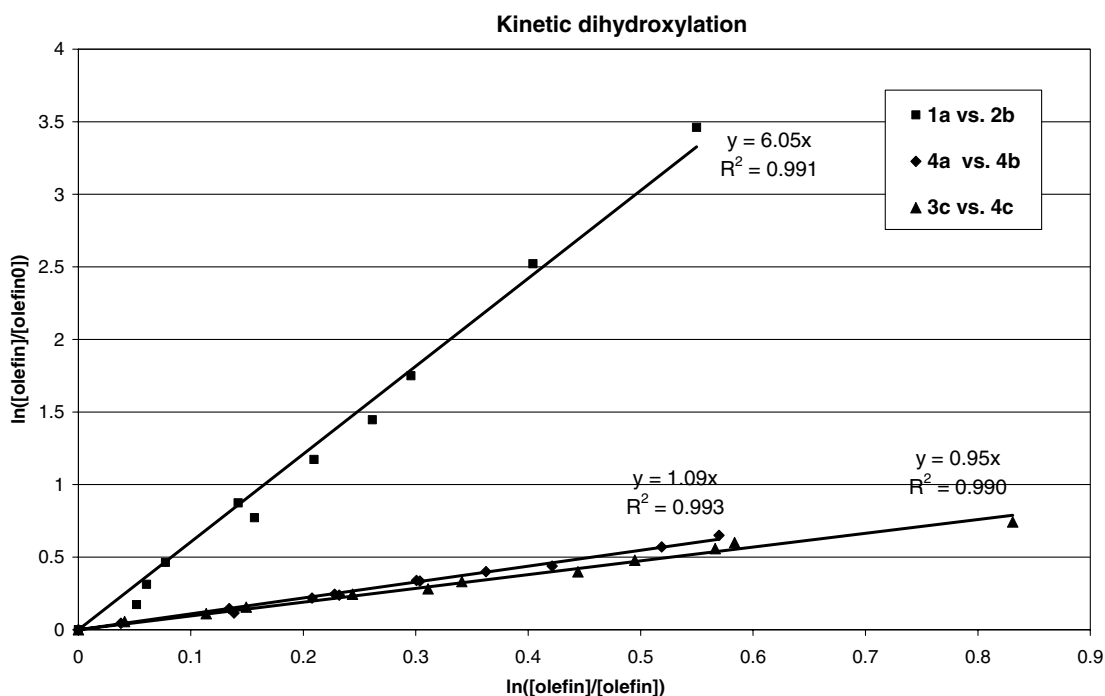


Fig. 11. The remaining kinetic dihydroxylation, which enable us to determine the relative reactivity of all 12 alkenes. Note that the competitive dihydroxylation collected in this plot have been performed using different reference compounds. Thus, the relative reactivity of the compounds within this plot cannot be assessed directly.

to the slowest reacting alkene **1c** is shown in a square next to each alkene, whereas the experimentally determined relative reactivity from each successful pair-wise competition is shown in an ellipse on the corresponding arrow.

Examining Fig. 12 in more detail one realizes that the largest difference in reactivity determined successfully was 10.8:1 measured between **3b** and **3c**. Multiplying with the reactivity of **3c** one arrives at a reactivity of 71.5 for **3b** relative to the reference compound **1c**. The accuracy of this

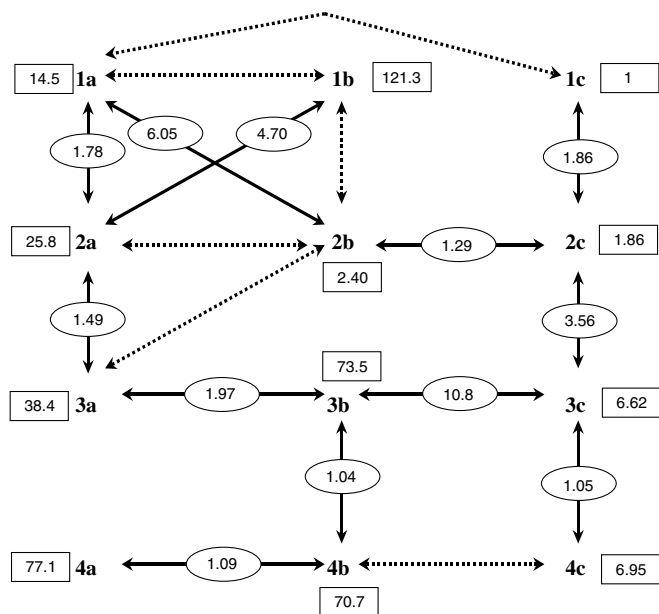


Fig. 12. Overview of the experimentally determined relative reactivities in the two-phase *t*-BuOH:H₂O system. A dotted arrow indicates the difference in reactivity was too large to be determined. A full arrow indicates a successful determination, with the relative reactivity shown in an ellipse.

determination can be assessed by following the path **3c** → **2c** → **2b** → **1a** → **2a** → **3a** arriving at **3b** now having a relative reactivity of 75.6 – a relative error of ca. 5%, which is acceptable considering the fact that six consecutive determinations of relative reactivity were used. A priori we cannot judge which of the two determinations is the most accurate one – a single determination of a relatively high reactivity (with an uncertain accuracy), or the use of six consecutive determinations each with relatively good accuracy. Consequently, in Fig. 12 we have chosen to show an average value of 73.5 for the reactivity of alkene **3b**.

Along with the kinetic dihydroxylations the resulting diols were synthesized using catalytic amounts of osmium

in *t*-BuOH:H₂O and the resulting ee was measured by chiral GC. In Table 1 is summarized experimental reactivity determined in toluene along with reactivity and selectivity (ee) in the two-phase *t*-BuOH:H₂O. It is interesting to note that, despite the fact that trisubstituted alkenes generally are considered favored substrates for the AD reaction, several of the substrates investigated here display moderate or even low enantioselectivity.

3. Computational methods

Force field modeling of transition states has been performed using the previously described Q2MM force field [14] for the AD reaction [11a], updated [13] to work with MacroModel v8.0 [17]. The results are not identical to the published force field [11a], but relative energies generally deviate only by 1–2 kJ/mol⁻¹. Conformational searches consisted of systematic Monte Carlo searches [18] of selected torsions as described previously [13] followed by a re-optimization in vacuo with a tight energy cutoff (20 kJ/mol⁻¹). The ensemble of conformations thus generated was used as a starting point for a mixed Monte-Carlo [19]/low mode [20] search which was performed for 100,000 steps. In the Monte Carlo part of the search the full set of torsions was now included. Finally, another reoptimization was performed either in vacuo or with the built-in solvation model for H₂O. These two sets of calculations represent two extremes. The experimental results were expected to lie in between these two sets, with the toluene results closer to gas phase, and the bi-phasic results (where the reaction probably occurs in the *t*-BuOH-phase) closer to the results obtained with the continuum model for water. Separate conformational searches were performed for each of the four possible approach vectors of the alkene [6,13], corresponding to the four possible orientations in the mnemonic device. When referencing individual ensembles, they are designated by which corner of the mnemonic the alkene hydrogen is pointing to. Thus, for all alkenes, from the mnemonic we would expect the energetically best ensemble to be the one designated SE. The free alkenes were subjected to systematic Monte Carlo searches [18] only, since these have few enough degrees of freedom so that it is possible to guarantee a complete coverage of the conformational space using a systematic search.

Ensemble energies for each conformational search are obtained by Boltzmann summation over all conformations according to Eq. (1), and thus include conformational entropy, but not vibrational or solvation contributions, unless included explicitly in each individual conformational energy. Note that Eq. (1) can also be used to combine several different ensembles (like those for all alkene orientations) into one global ensemble

$$E = -RT \ln \left(\sum_i e^{-E_i/RT} \right). \quad (1)$$

Table 1

Experimentally determined reactivities and enantioselectivities for the dihydroxylation of all 12 alkenes

Alkene	k_{rel} (experimental) ^a		ee (%) exp
	Toluene	<i>t</i> -BuOH:H ₂ O	
1a	12.1	14.4	96.4
1b	45.3	119.5	99.8
1c	1	1	72.6
2a	9.3	13.8	97.6
2b	1.40	1.29	28.0
2c	1	1	21.3
3a	2.37	5.8	95.6
3b	2.58	11.3	89.0
3c	1	1	49.4
4a	3.53	11.3	96.7
4b	3.06	10.4	94.2
4c	1	1	46.4

^a Reactivities (k_{rel}) relative to alkene **c** in each group of isomers.

Enantioselectivities are calculated by combining all paths contributing to one enantiomer into one ensemble using Eq. (1), and are reported as relative activation barriers. The enantiomeric ratio (er) and ee can then be calculated using Eqs. (2) and (3). The calculation of ee is defined to yield a positive number if the major enantiomer is obtained from the expected SE orientation of the alkene in the mnemonic device, that is, the energy for the ensemble containing the SE (and NW) conformations is lowest in energy

$$\text{er} = e^{(E_{\text{SW+NE}} - E_{\text{SE+NW}})/RT}, \quad (2)$$

$$\text{ee} = \frac{\text{er} - 1}{\text{er} + 1}. \quad (3)$$

Relative rates must be obtained isodesmically. As in our previous work [13], the competition is seen as a pseudo-equilibrium where the alkene in one TS exchanges with free alkene to form an alternative TS. The relative activation energy can then be obtained from Eq. (4), where E in all cases corresponds to total ensemble energies obtained from all contributing conformations for one type of TS or alkene. We define the reference alkene as alkene 1, so that Eq. (4) always yields a positive number for any alkene that reacts faster than the reference (alkene **c** in each group, or **1c** globally). We note that when the two products in the competition are more different than simple stereoisomers (i.e., for all comparisons except between **b** and **c** within each group), the isodesmic comparison is not isoparametric, which means that systematic errors present in all molecular mechanics treatments do not necessarily cancel. Thus, we will also be testing the importance of the systematic errors in our force field for an isodesmic comparison

$$\Delta\Delta E^\ddagger = E_{\text{TS1}} - E_{\text{TS2}} - E_{\text{alkene1}} + E_{\text{alkene2}}. \quad (4)$$

4. Computational results

The calculated relative rates of dihydroxylation of all alkenes relative to alkene **c** within each group are shown in Table 2.

In all cases the **a** and **b** alkenes react faster than the **c** alkenes due to the stabilizing interactions with the ligand environment. This stabilization also accounts for the correlation between selectivity and rate, which is a general fea-

Table 2
Calculated values for the differences in activation energy within each isomeric group of alkenes (Eq. (4))

Group	$\Delta\Delta E^\ddagger$ calc (kJ/mol)			
	In vacuo		H ₂ O	
	a	b	a	b
1	12.1	12.3	10.5	9.0
2	12.2	2.9	10.8	2.9
3	4.3	3.7	3.2	2.9
4	4.6	5.6	5.1	2.5

The **c** alkene within each group has been used as reference.

ture in the AD reaction [3]. Looking at the results in Table 2, two features are striking. Firstly, the reactivity span is much wider for alkenes **1** and **2** than for **3** and **4**. We attribute this mainly to a difference in the reactivity of the respective reference alkenes **c**, which have tethers long enough to allow the alkene to fold the phenyl group into attractive areas of the ligand, irrespective of the actual attachment point of the tether. Secondly, the benzyl-substituted alkenes **2** are unique in that there is a large difference between the reactivity of **2a** and **2b**. Since this difference can also be seen in the experimental data (Fig. 5), we decided to look in more detail at the most favorable paths for dihydroxylation of **2b**.

The most surprising feature of the transition states for **2b** is that the orientation which was expected to be favored based on the mnemonic device, SE (which has the benzyl group oriented into the SW corner), is found to be isoenergetic with the NE orientation, where the benzyl group points into the non-interacting NW corner and a methyl group is positioned into the sterically crowded SE corner. The reason for this can be found in the exact orientation of the benzyl group in the pocket created by the quinolines. This pocket is well suited for a phenyl group directly attached to the reacting alkene, but the intervening methylene in **2b** requires that the direction of the phenyl group of **2b** differs by ca 70° from that of the phenyl group in **1b**. The fairly narrow cleft defined by the two quinolines cannot accommodate this drastic change in orientation. When the ligand is forced to accept a benzyl group in this cleft, it undergoes a conformational change which allows it to interact favorably with the benzyl group, but at the cost of a high conformational energy (Fig. 13, left).

The best possible conformation of **2b** can instead be found in the NW orientation, with the benzyl group pointing towards the NE corner (Fig. 13, right). In this orientation, the benzyl group can be stabilized by the PHAL linker, which provides a much more open, L-shaped pocket [9], but at the cost of having to point a methyl group into the crowded SE corner, rationalizing the low reactivity of **2b**.

Interestingly, the SW orientation, with the benzyl group pointing into the sterically crowded SE corner (Fig. 14), was found to be only 3 kJ/mol higher in energy than the best conformation, the NW orientation shown in Fig. 13. On analyzing the structure, we see that the auxiliary alkaloid unit has undergone a drastic change of orientation to achieve some stabilizing interactions with the benzyl substituent at only a moderate steric cost. Since this orientation leads to the opposite enantiomer compare to the favored NW orientation, a very low ee is expected for **2b**, in good agreement with the experimental data (Table 1).

For the **c** alkenes neither of the four possible orientations of the alkene within the osmium–ligand complex are especially favored, but as expected from previous work, we can see that the long tethers of alkenes **3c** and **4c** indeed allow the alkene to fold and put the phenyl group in close proximity to various parts of the ligand. The folded conformers suffer a penalty of a few kJ/mol due to gauche

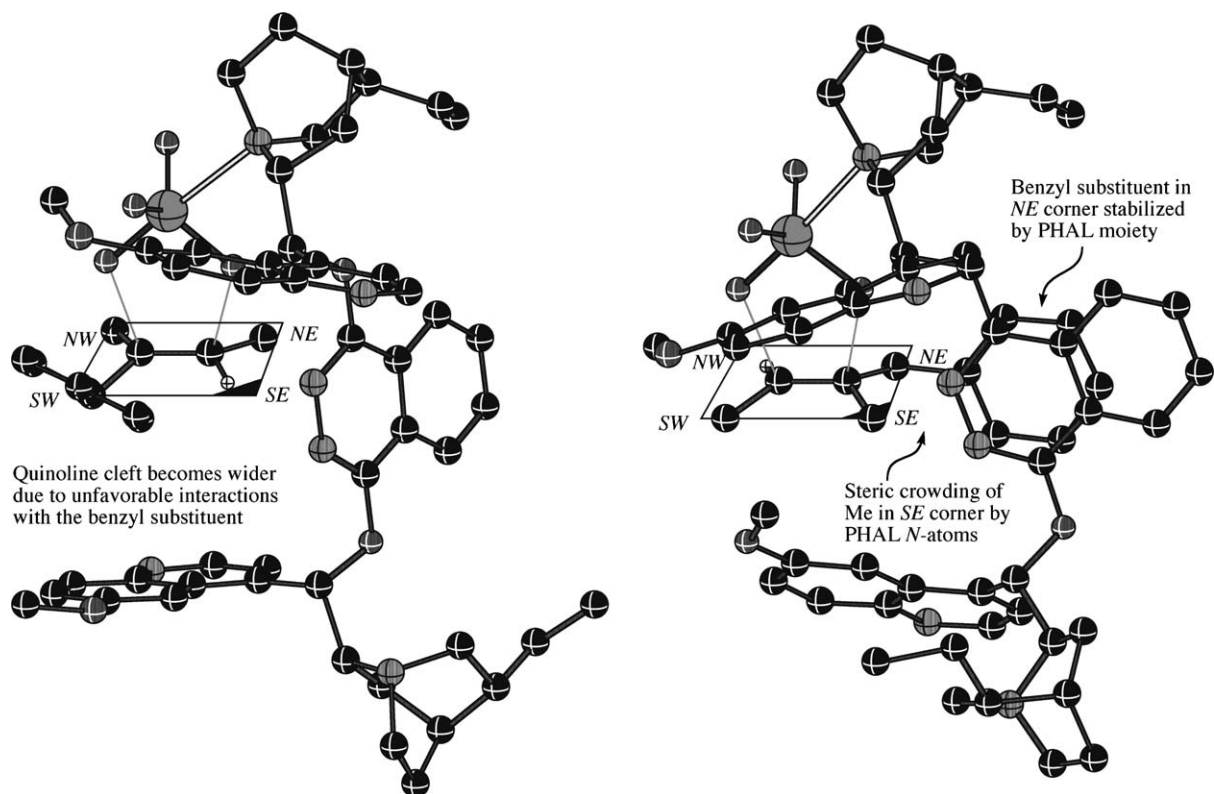


Fig. 13. Left: The best SE orientation of **2b**. Right: The best TS structure for **2b**, the NW orientation, with the benzyl group stabilized by the PHAL moiety in the NE corner.

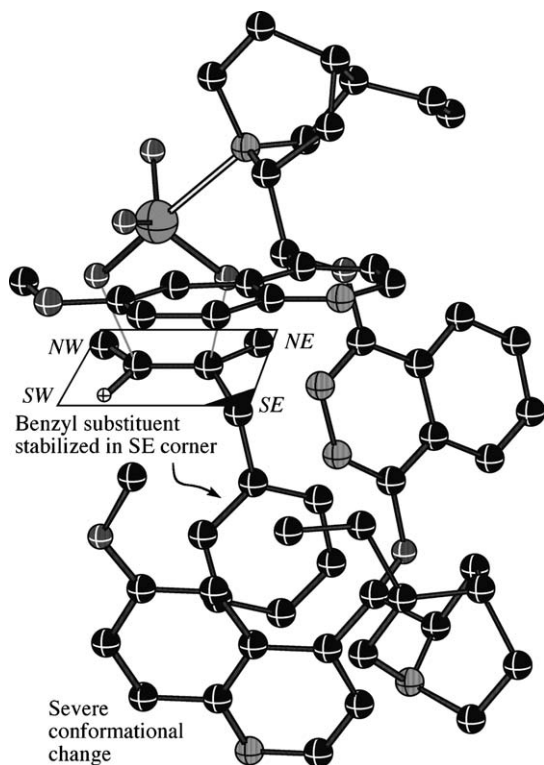


Fig. 14. The SW orientation of **2b**, with the benzyl group in the SE corner, crowded by the PHAL moiety.

interactions, but also some gain due to conformational entropy. In other words, several slightly stabilized conformations are possible for the **c** alkenes, whereas only a few highly stabilized conformations can be achieved in the ligand pockets of the SW and NE corners.

As a final point on the results in Table 2, we can see that utilization of a computational solvation model leads to a small but systematic decrease in rate differences. This is entirely in line with expectations, since the surface area available for stabilization by the solvent is largest for alkenes **c**, where the large group is mostly pointing out into the solvent.

Turning now to enantioselectivities, the calculated results are shown as relative activation barriers in Table 3. Numbers are shown as positive for all cases where the calculated major enantiomer corresponds to what would be predicted from the mnemonic devices (in all cases orientation SE). We first note that the solvation model has little effect on calculated enantioselectivities, as expected for the AD reaction where ee values measured in water and toluene usually differ by only a few percent [3]. The target accuracy of the Q2MM method is around 2 kJ/mol [11a]; differences lower than this are considered to be within the uncertainty of the method. We can immediately see that only two substrates, **1a** and **1b**, are expected to yield very high enantioselectivities. For the remaining substrates,

Table 3
Calculated values for the differences in activation energies for the diastereomeric transition states leading to opposite enantiomers

Group	$\Delta\Delta E^\ddagger$ calc (kJ/mol)					
	In vacuo			H ₂ O		
	a	b	c	a	b	c
1	13.1	14.2	3.3	13.0	11.9	2.0
2	4.8	3.1	-1.8	6.9	5.7	0.9
3	7.4	7.4	1.5	8.3	7.2	2.2
4	7.6	7.2	-0.8	8.9	5.2	0.6

where the longer tethers allow stabilization of several orientations, the difference between competing paths is smaller, and largely arises from the steric crowding of single methyl groups in the SE corner for orientations leading to the minor enantiomer. For the alkenes **c**, we can even see that the absolute stereochemistry of the major enantiomer is uncertain. In terms of orientation in the mnemonic device, this is due to the fact that there is a competition between on the one hand orientation SE, which experiences neither steric penalty nor attractive interactions, and on the other hand orientations SW and NE, where an attractive interaction can be obtained, but at the cost of a steric clash between a methyl group and the PHAL linker in the SE corner. For alkenes **2c** and **4c**, the prediction of absolute stereochemistry is even dependent on whether a solvent model is used or not, but since all of the corresponding energies are within 2 kJ/mol, the predictions must all be considered to be inconclusive in view of the expected uncertainty of our method.

5. Comparison between theory and experiment

Computational results are initially obtained as energies, which can later be converted to experimental observables for direct comparison to experimental numbers. However, properties like reaction rates are exponentially dependent on the energies, with the result that an error in the calculated property is a non-linear function of the underlying

Table 4
The experimental reactivities and selectivities converted to differences in activation energy

Group	$\Delta\Delta E^\ddagger$ exp (kJ/mol)						
	Toluene		<i>t</i> -BuOH:H ₂ O		ee		
	a	b	a	b	a	b	
Isomer:	a	b	a	b	a	b	c
1	6.2	9.4	6.6	11.9	9.9	>17 ^a	4.6
2	5.5	0.8	6.5	0.6	10.9	1.4	1.1
3	2.1	2.3	4.4	6.0	9.4	7.0	2.7
4	3.1	2.8	6.0	5.8	10.1	8.7	2.5

^a Only the major enantiomer was observed and consequently the ee was assumed to be at least 99.8%.

energy. For example, an error of 2 kJ/mol is approximately equal to the difference between 0% and 30% ee at room temperature, but also to the difference between 98% and 99% ee. To investigate the correlation between experimental and computational results, it is usually more appropriate to convert the former to energies, and then compare those to the computational data. The data from Table 1 have therefore been converted to relative activation energies for the two competing process, Table 4.

The experimental differences in activation energy obtained in toluene were plotted against the theoretical values obtained in vacuo (Fig. 15).

Each data point corresponds to one of the eight **a** or **b** substrates – the **c** alkenes are left out since they are used as reference compounds within each group and thus assigned a relative reactivity of 1. The correlation is good, with only two values deviating more than 2 kJ/mol from the regression line. Interestingly, we see no significant difference in performance for the **a** and **b** series, despite the fact that the isodesmic comparison is fully isoparametric only for the **b** series. It therefore seems that the systematic errors in bending and torsion functions that are not fully compensated in the **a** vs. **c** comparison give an insignificant contribution to the error in the current study. However, if bond types change (as in a comparison of **1a** vs. **2a**), the molecular mechanics comparison is no longer valid, since

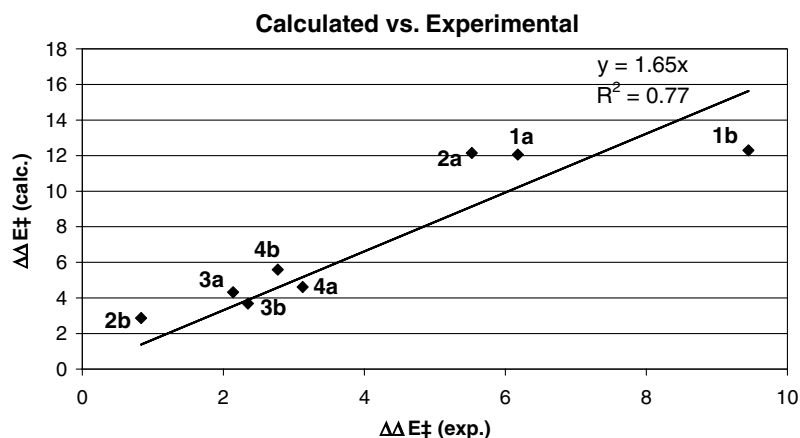


Fig. 15. Activation energies relative to the **c** alkenes, computational results in vacuo vs. experimentally determined values in toluene.

the unknown systematic errors connected to bond type changes and varying degrees of conjugation are significant.

The slope in Fig. 15 is significantly higher than 1, indicating that energy differences are systematically overestimated by the force field. We can see two obvious sources for this systematic error. It is a known deficiency of the Q2MM methodology that, even though distortions perpendicular to the reaction coordinate are handled well by the force field, changes along the reaction coordinate cannot be correctly represented [14]. In real systems, the system can relax along the reaction coordinate in response to steric and electronic changes, whereas in the current Q2MM implementation, the reaction coordinate is in effect frozen. This naturally leads to a steep energy increase in the model, where the real system might have the possibility for a soft relaxation. The second possibility is that the non-bonded interactions responsible for the steric attraction, and therefore for the difference between the various orientations, have less influence in solvent. An indication of the relative importance of these two factors can be obtained from a

comparison with the results obtained using a computational solvation model. We decided to make this comparison for the experimental data obtained in the two-phase *t*-BuOH:H₂O system which are plotted against the calculated values in vacuo in Fig. 16 and against data from the solvated calculations in Fig. 17.

With the experimental data from the two-phase system, the correlation is significantly worse than for the toluene data, but interestingly the slope is now close to 1. Furthermore, the slope is smaller for the calculations employing the solvation model, indicating that a part of the systematic error in Fig. 15 is due to an overestimation of the non-bonded interactions. However, the larger errors in the two-phase system preclude a full assignment of the source of the systematic error. We also note that the experimental system, which contains a high concentration of salts, may not be well represented by either the gas phase or the water model calculations. To conclude the comparison of relative rates, for the reaction in non-polar solvent, we obtain a good correlation between calculated and experimental

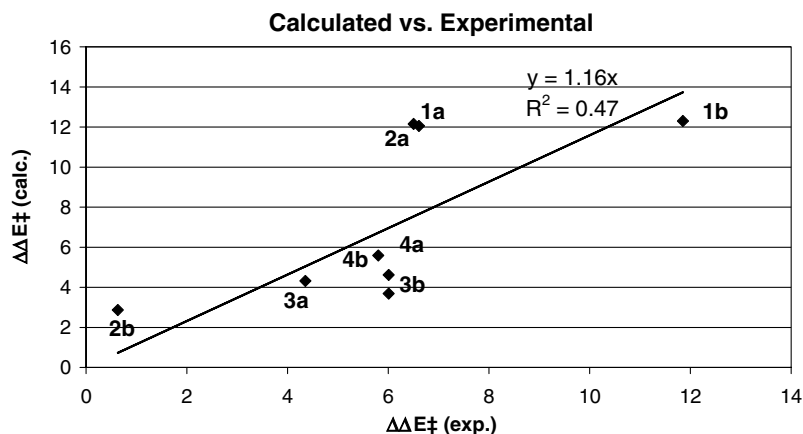


Fig. 16. The calculated differences in activation energies (in vacuo) relative to the c compounds against the experimentally determined values in the two-phase *t*-BuOH:H₂O system.

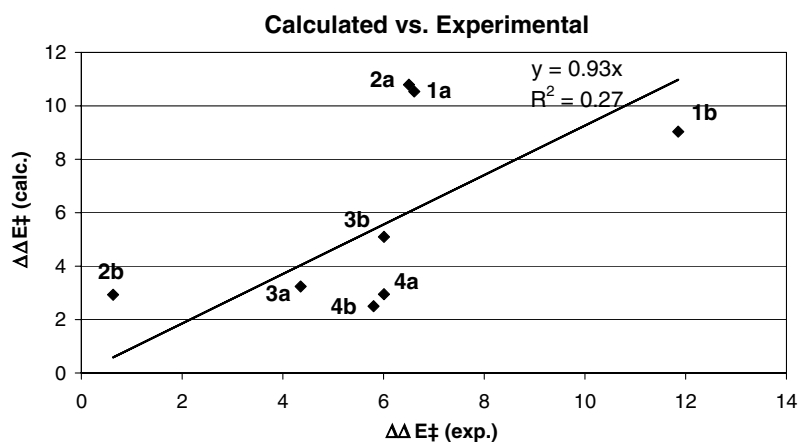


Fig. 17. The calculated differences in activation energies (in water) relative to the c compounds against the experimentally determined values in the two-phase *t*-BuOH:H₂O system.

data. For reactions in polar solvent, the errors are still small in an absolute sense, but too large to allow a truly predictive model for relative reactivity.

For the determination of *ee*, the error in terms of energy is expected to be smaller since the comparison is now between diastereomeric structures, and furthermore, the systematic errors which may affect the results when using molecular mechanics calculations for comparing isomers should cancel completely when comparing diastereomers. We therefore plot the calculated versus the experimental results without performing a regression. The dotted line instead symbolises perfect agreement (slope = 1). Since the absolute stereochemistry has not yet been determined for the previously unknown products in the current study, the energy derived from the experimental data is assumed to be positive, that is, that all alkenes give the major product predicted from the mnemonic device. For some of the products displaying very low *ee*, this assumption may be false, but will not have a major impact on the following discussion. The enantioselectivities in the current study have been determined for the products obtained from the two-phase *t*-BuOH:H₂O system. The experimentally derived energies

are plotted against the data calculated in vacuo in Fig. 18, and against the data calculated in solvent in Fig. 19.

The agreement is very good, with most of the computational predictions falling within the target accuracy, 2 kJ/mol. The agreement is slightly worse in the calculations employing the solvation model, despite the fact that the experimental data were obtained in a polar solvent, indicating that in this case, the solvation introduces a slightly higher level of random noise in the calculations, and does not correct for any significant systematic errors.

The largest error obtained is for the benzyl-substituted alkene **2a**. The absolute value of the error is still fairly small, ca 4 kJ/mol for the in vacuo calculations and 6 kJ/mol employing the water model, and might therefore just represent the extreme of a random distribution of errors. However, we also wish to point out that the derivation of the original Q2MM force field [11a] included quantum chemical data for reactions of phenyl- and alkyl-substituted alkenes, but no benzyl-substituted alkenes. It is therefore plausible that torsional parameters for the bond connecting the benzyl group to the reacting alkene, which should be subject to hyperconjugation effects unique

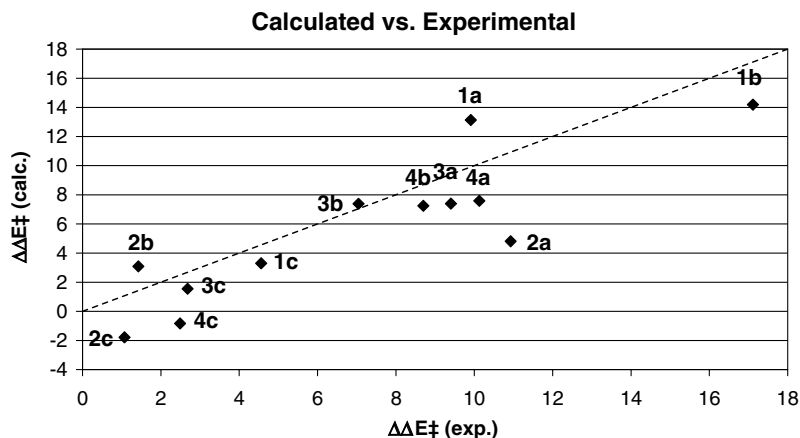


Fig. 18. Calculated enantioselectivities in vacuo plotted against the experimentally determined enantioselectivities.

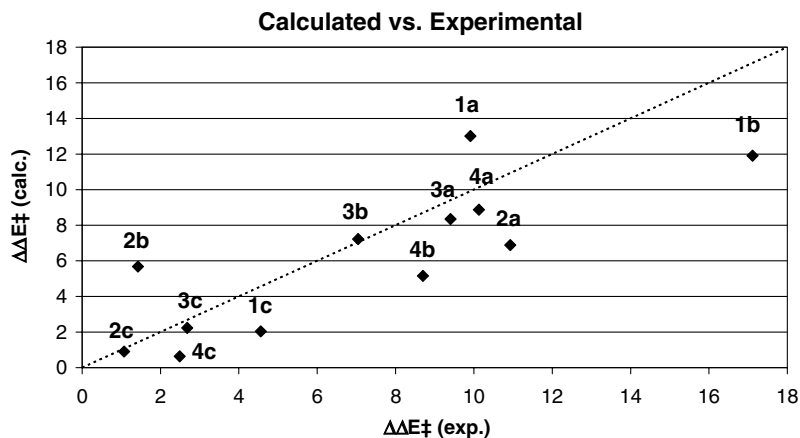


Fig. 19. Calculated enantioselectivities using the water model plotted against the experimentally determined enantioselectivities.

to the benzyl moiety, have been improperly implemented in the current force field, leading to incorrect orientations of the benzyl group in the chiral pockets of the ligand.

In view of the generally excellent agreement between the calculated and experimental selectivities reported here and previously [11a], we have analyzed the interactions in several of the most important conformations of the transition states in the current study. Our findings are summarized in Fig. 20, where the best transition state for the dihydroxylation of **1b** has been overlaid on our revised mnemonic device. To summarize, the strongest selectivity-determining interactions come from the PHAL linker, which is responsible for the steric crowding of the point in space corresponding to the SE corner of the mnemonic device. It is important to note that this interaction has been present in all successful ligands for the AD reaction. Even the acetate used in the first report by Hentges and Sharpless [1] prefers a conformation where the carbonyl carbon is virtually superimposable on one of the PHAL nitrogen atoms.

Another important contribution of the PHAL is to provide attractive stabilization to substituents pointing into the NE corner of the mnemonic device. In conjunction with the backside of the quinuclidine coordinating to Os, the PHAL moiety forms an L-shaped pocket which is able to accommodate a wide range of substituent shapes. It is

unique in that all substituents in the current study can be stabilized in this pocket (alkenes **a**).

The auxiliary quinoline moiety (on the alkaloid unit which does not coordinate to Os) also has two important functions. Firstly, it stabilizes the back-side of the reacting alkene, providing a energy bonus for reaction involving the equatorial oxygen pointing into the pocket. This interaction can truly be described as a π - π -interaction, since the electrons of the π -system of the quinoline presumably stabilize the σ^* -orbital of the forming C–O bond. The interaction is also electrostatic in nature; population analysis of quantum chemical transition states has revealed significant positive charge on the alkene carbons in the transition state. Secondly, both quinolines form a cleft which can stabilize certain alkene substituents in the SW corner of the mnemonic device. It is obvious that this stabilization is strongly dependent on shape, since the benzyl moiety could not be accommodated (alkene **2b**), whereas all other alkenes in the **b** series experience stabilization in this cleft. The quinoline on the primary alkaloid unit participates in some of this stabilization, and also provides significant dipole stabilization of the complex by interaction between the MeO-substituent and the axial oxo-group.

6. Summary

The revised mnemonic [13] for the AD reaction has been validated by a broad substrate selectivity study, and the limitations of this qualitative prediction tool have been pointed out. Several of the substrates investigated here should yield good enantioselectivities according to the mnemonic, but in fact give only low to moderate selectivity. We have verified that our Q2MM force field [11a] for the AD-reaction provides excellent results for prediction of enantioselectivities, and fair correlation with relative reactivities of different substrates if the comparison is performed isodesmically. The latter point is surprising in view of the known deficiencies in empirical force fields for comparisons of substrates with different bonding patterns. The influence of each moiety of the PHAL ligand on the rate and selectivity of the AD-reaction has been elucidated.

7. Experimental

7.1. General

EtOAc and hexane for chromatography were distilled under nitrogen. THF was distilled from Na/benzophenone under nitrogen. Purification of crude products was done by flash column chromatography on Matrex 60 Å silica gel. All moisture-sensitive reactions were performed in flame-dried glassware under argon. Optical rotations were measured on a Perkin–Elmer 241 polarimeter at 589 nm (CH_2Cl_2). ^1H and ^{13}C NMR spectra were obtained using a Varian Mercury300 operating at 300 and 75 MHz, respectively. MS (electron impact) was performed on VG Masslab Trio-2. GC-HRMS was performed on a Waters

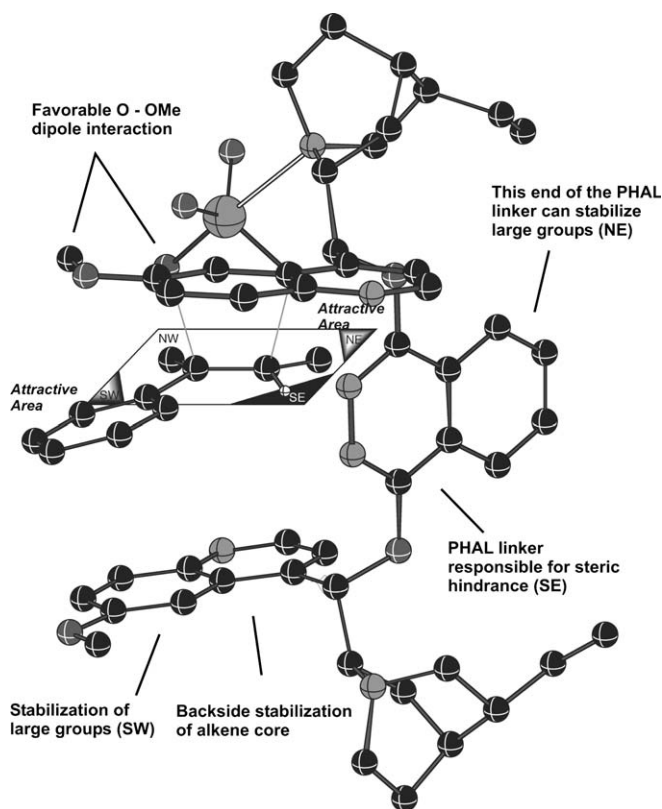


Fig. 20. The global minimum structure of alkene **1b** with the phenyl group stabilized in the south-west corner has been overlaid on the revised mnemonic device. The most important stabilizing interactions have been mapped.

Micromass GCT equipped with an Agilent DB-5MS column.

7.2. Synthesis

Alkenes **1a–c** were synthesized using an adapted Suzuki-Miyaura cross-coupling procedure catalyzed by palladium(0) [21–23] as reported previously [13]. The gem-substituted alkene **2a** was synthesized by a Wittig reaction between acetone and the appropriate phosphonium salt and isolated as a clear oil after chromatography in 16% yield [24]. ^1H NMR (CDCl_3) 1.73 (s, 3H, CH_3), 1.75 (s, 3H, CH_3), 3.35 (d, 7.5 Hz, 2H, Ph- CH_2), 5.34 (m, 1H, =C-H), 7.15–7.35 (m, 5H, aryl-H). ^{13}C NMR (CDCl_3) 18.1 (1C, CH_3), 26.0 (1C, CH_3), 34.7 (1C, CH_2), 123.5, 125.9, 128.5, 128.6 (6C, aromatic carbons), 132.7 (1C, =C-H), 142.1 (1C, =C). m/z (EI): 147 (6%, $[\text{M} + 1]^+$), 146 (51%, M^+), 131 (100%, $[\text{M} - \text{CH}_3]^+$), 91 (50%, $\text{C}_6\text{H}_5\text{CH}_2^+$). Exact mass calculated for $\text{C}_{11}\text{H}_{14}$: 146.1096, found 146.1099.

The alkenes **2b** and **2c** were synthesized from the vinyl bromides as follows: THF (100 mL) was cooled to -78°C . The vinyl bromide was added followed by slow addition of two equivalents of *t*-BuLi. After 1 h, 1.1 equivalents of CuCN was added. Finally, 1.1 equivalents of benzyl bromide was added slowly and the reaction mixture was kept at -40°C while being monitored by TLC ($R_f(\text{BnBr}) = 0.20$, $R_f(\text{vinyl bromide}) = 0.28$ and $R_f(\text{alkene}) = 0.48$ all in hexane). The reaction was quenched with sat. aq. NH_4Cl followed by standard workup. (*E*)-2-Methyl-1-phenyl-2-butene (**2b**, 10.6 mmol scale) was isolated as a clear oil in 44% yield (4.3 mmol, 684 mg) ^1H NMR (CDCl_3) 1.56 (s, 3H, CH_3), 1.63 (d, 6.6 Hz, 3H, CH_3), 3.30 (s, 2H, Ph- CH_2), 5.32 (m, 1H, =C-H), 7.15–7.35 (m, 5H, aryl-H). ^{13}C NMR (CDCl_3) 13.5 (1C, CH_3), 15.5 (1C, CH_3), 46.2 (1C, CH_2), 120.4, 125.8, 128.1, 128.8 (6C, aromatic carbons), 135.1 (1C, =C), 140.5 (1C, =C). m/z (EI): 147 (6%, $[\text{M} + 1]^+$), 146 (50%, M^+), 131 (100%, $[\text{M} - \text{CH}_3]^+$), 91 (96%, $\text{C}_6\text{H}_5\text{CH}_2^+$). Exact mass calculated for $\text{C}_{11}\text{H}_{14}$: 146.1096, found 146.1098.

(*Z*)-2-Methyl-1-phenyl-2-butene (**2c**, 22.7 mmol scale) was isolated as a clear oil in 68% yield (14.0 mmol, 2.247 g). ^1H NMR (CDCl_3) 1.62 (s, 3H, CH_3) 1.72 (d, 6.9 Hz, 3H, CH_3), 3.38 (s, 2H, Ph- CH_2), 5.40 (m, 6.9 Hz, 1H, =C-H), 7.35–7.15 (m, 5H, aryl-H). ^{13}C NMR (CDCl_3) 13.7 (1C, CH_3), 23.3 (1C, CH_3), 37.5 (1C, CH_2), 120.3, 125.8, 128.3, 128.5 (6C, aromatic carbons), 134.7 (1C, =C), 140.3 (1C, =C). m/z (EI): 147 (5%, $[\text{M} + 1]^+$), 146 (48%, M^+), 131 (100%, $[\text{M} - \text{CH}_3]^+$), 91 (94%, $\text{C}_6\text{H}_5\text{CH}_2^+$). Exact mass calculated for $\text{C}_{11}\text{H}_{14}$: 146.1096, found 146.1101.

Alkenes **3a–c** were synthesized using an one-pot hydroboration – Suzuki-Miyaura cross-coupling procedure [13]. The fourth group of alkenes (**4a–c**) were synthesized in a similar manner using allylbenzene instead of styrene in the first hydroboration step. In all three reactions 4.4 mmol allylbenzene, 4.4 mmol 9-BBN, 4.0 mmol of the appropri-

ate vinyl bromide and 2 mol% of the $\text{Pd}(\text{PPh}_3)_4$ catalyst were used.

2-Methyl-6-phenyl-2-hexene (**4a**) was isolated as a clear oil in 46% yield (1.86 mmol) after chromatography. ^1H NMR (CDCl_3) 1.64 (s, 3H, CH_3), 1.65–1.75 (m, 2H, CH_2), 1.75 (d, 1.2 Hz, 3H, CH_3), 2.06 (q, 7.3 Hz, 2H, CH_2), 2.65 (t, 7.8 Hz, 2H, CH_2), 4.55 (m, 1H, =C-H), 7.15–7.35 (m, 5H, aryl-H). ^{13}C NMR (CDCl_3) 17.7 (1C, CH_3), 25.7 (1C, CH_3), 27.7 (1C, CH_2), 31.6 (1C, CH_2), 35.5 (1C, CH_2), 124.3, 125.5, 128.2, 128.4 (6C, aromatic carbons), 131.7 (1C, =C), 142.7 (1C, =C). m/z (EI): 175 (5%, $[\text{M} + 1]^+$), 174 (38%, M^+), 118 (20%, $[\text{Ph}-\text{CH}_2-\text{CH}=\text{CH}]^+$), 117 (25%, $[\text{Ph}-\text{CH}_2-\text{CH}=\text{C}]^+$), 105 (42%, $[\text{Ph}-\text{CH}_2-\text{CH}_2]^+$), 104 (100%, $[\text{Ph}-\text{CH}_2-\text{C}]^+$), 92 (52%, $[\text{Ph}-\text{CH}_3]^+$), 91 (69%, $[\text{Ph}-\text{CH}_2]^+$), 69 (36%, $[(\text{CH}_3)_2\text{C}=\text{CH}-\text{CH}_2]^+$), 55 (42%, $[(\text{CH}_3)_2\text{C}=\text{CH}]^+$), 41 (63%, $[(\text{CH}_3)\text{C}=\text{CH}_2]^+$). Exact mass calculated for $\text{C}_{13}\text{H}_{18}$: 174.1409, found 174.1411.

(*E*)-3-Methyl-6-phenyl-2-hexene (**4b**) was isolated as a clear oil in 60% yield (2.41 mmol) after chromatography. ^1H NMR (CDCl_3) 1.60 (d, 7.5 Hz, 3H, CH_3), 1.61 (s, 3H, CH_3), 1.68–1.80 (m, 2H, CH_2), 2.09 (t, 7.7 Hz, 2H, CH_2), 2.61 (t, 7.8 Hz, 2H, CH_2), 5.24 (m, 1H, =C-H), 7.15–7.35 (m, 5H, aryl-H). ^{13}C NMR (CDCl_3) 13.3 (1C, CH_3), 15.8 (1C, CH_3), 29.9 (1C, CH_2), 35.8 (1C, CH_2), 39.5 (1C, CH_2), 118.8, 125.8, 128.4, 128.6 (6C, aromatic carbons), 135.7 (1C, =C), 143.0 (1C, =C). m/z (EI): 174 (5%, M^+), 117 (2%, $[\text{Ph}-\text{CH}_2-\text{CH}=\text{C}]^+$), 105 (15%, $[\text{Ph}-\text{CH}_2-\text{CH}_2]^+$), 104 (100%, $[\text{Ph}-\text{CH}_2-\text{C}]^+$), 92 (7%, $[\text{Ph}-\text{CH}_3]^+$), 91 (17%, $[\text{Ph}-\text{CH}_2]^+$), 55 (15%, $[(\text{CH}_3)_2\text{C}=\text{CH}]^+$), 41 (17%, $[(\text{CH}_3)\text{C}=\text{CH}_2]^+$). Exact mass calculated for $\text{C}_{13}\text{H}_{18}$: 174.1409, found 174.1411.

(*Z*)-3-Methyl-6-phenyl-2-hexene (**4c**) was isolated as a clear oil in 47% yield (1.90 mmol) after chromatography. ^1H NMR (CDCl_3) 1.64 (d, 6.9 Hz, 3H, CH_3), 1.70 (s, 3H, CH_3), 1.70–1.80 (m, 2H, CH_2), 2.09 (t, 7.8 Hz, 2H, CH_2), 2.61 (t, 7.8 Hz, 2H, CH_2), 5.24 (m, 1H, =C-H), 7.15–7.35 (m, 5H, aryl-H). ^{13}C NMR (CDCl_3) 13.6 (1C, CH_3), 23.6 (1C, CH_3), 29.8 (1C, CH_2), 31.3 (1C, CH_2), 36.0 (1C, CH_2), 119.5, 125.9, 128.5, 128.6 (6C, aromatic carbons), 136.0 (1C, =C), 142.9 (1C, =C). m/z (EI): 174 (7%, M^+), 117 (2%, $[\text{Ph}-\text{CH}_2-\text{CH}=\text{C}]^+$), 105 (17%, $[\text{Ph}-\text{CH}_2-\text{CH}_2]^+$), 104 (100%, $[\text{Ph}-\text{CH}_2-\text{C}]^+$), 92 (8%, $[\text{Ph}-\text{CH}_3]^+$), 91 (19%, $[\text{Ph}-\text{CH}_2]^+$), 55 (12%, $[(\text{CH}_3)_2\text{C}=\text{CH}]^+$), 41 (12%, $[(\text{CH}_3)\text{C}=\text{CH}_2]^+$). Exact mass calculated for $\text{C}_{13}\text{H}_{18}$: 174.1409, found 174.1411.

8. General dihydroxylation procedure

The dihydroxylation and characterization of the diols **5a–c** and **7a–c** have been reported earlier [13]. The synthesis of the diols **6a–c** and **8a–c** was performed in a similar manner. In order to allow determination of enantiomeric purity by GC the diols **6–8** were derivatized as follows. To ~ 1 mg of diol in a small vial was added one drop of pyridine and two drops of acetic anhydride. The vial was closed and heated to 100°C for two hours. The resulting mixture of

acetate and excess reagent was diluted with ~1 mL of EtOAc and analyzed by chiral-GC. The racemic diols were synthesized using quinuclidine as ligand for osmium and derivatized in a similar manner to validate the method. The racemates had identical ^1H and ^{13}C , but in some cases the physical appearance was different (see below).

(2*R*)-3-Methyl-1-phenyl-2-butane diol (**6a**) was isolated as colorless crystals in quantitative yield; m.p. 72–74 °C. ^1H NMR (CDCl_3) 1.24 (s, 3H, CH_3), 1.27 (s, 3H, CH_3), 2.22 (br s, 2H), 2.56 (dd, 13.5 Hz, 10.8 Hz, 1H), 2.88 (dd, 13.5 Hz, 2.1 Hz, 1H), 3.59 (dd, 10.8 Hz, 2.1 Hz, 1H), 7.20–7.37 (m, 5H, aryl-H). ^{13}C NMR (CDCl_3) 23.7 (1C, CH_3), 26.4 (1C, CH_3), 38.3 (1C, CH_2), 72.6 (1C, C–OH), 79.1 (1C, C–OH), 126.4, 128.6, 129.2, 138.9 (6C, aromatic carbons). $[\alpha]_{\text{D}}^{20} = 56.0$ ($c = 1.5$, CH_2Cl_2). Enantiomeric excess was measured to 97.6% by analysis of the acetate. Anal. found: C, 73.34; H, 9.08. Calc. for $\text{C}_{11}\text{H}_{16}\text{O}_2$: C, 73.30; H, 8.95%. The racemate was isolated as a yellow, amorphous solid in quantitative yield; m.p. 60–61 °C.

(2*R*,3*R*)-2-Methyl-1-phenyl-2-butane diol (**6b**) was isolated as a colorless solid in quantitative yield; m.p. 57–59 °C. ^1H NMR (CDCl_3) 1.09 (s, 3H, CH_3), 1.22 (d, 6.3 Hz, 3H, CH_3), 1.82 (br s, 1H, OH), 2.18 (br s, 1H, OH), 2.80 (s, 2H, CH_2), 3.67 (q, 6.3 Hz, 1H, CH), 7.20–7.40 (m, 5H, aryl-H). ^{13}C NMR (CDCl_3) 17.4 (1C, CH_3), 21.0 (1C, CH_3), 45.0 (1C, CH_2), 72.3 (1C, C–OH), 74.8 (1C, C–OH), 126.5, 128.2, 130.5, 136.9 (6C, aromatic carbons). $[\alpha]_{\text{D}}^{20} = 4.5$ ($c = 2.8$, CH_2Cl_2). Enantiomeric excess was measured to 28.0% by analysis of the acetate. Anal. found: C, 73.53; H, 9.00. Calc. for $\text{C}_{11}\text{H}_{16}\text{O}_2$: C, 73.30; H, 8.95%. The racemate was isolated as a colorless solid in 90% yield; m.p. 57–59 °C.

(2*R*,3*S*)-2-Methyl-1-phenyl-2-butane diol (**6c**) was isolated as a colorless solid in 91% yield; m.p. 73–75 °C. ^1H NMR (CDCl_3) 1.09 Hz (s, 3H, CH_3), 1.26 (d, 6.3 Hz, 3H, CH_3), 1.70 (br s, 1H, OH), 2.21 (br s, 1H, OH), 2.62 (d, 13.5 Hz, 1H, CH_2), 3.00 (d, 13.5 Hz, 1H, CH_2), 3.74 (q, 6.3 Hz, 1H, CH), 7.20–7.40 (m, 5H, aryl-H). ^{13}C NMR (CDCl_3) 17.2 (1C, CH_3), 23.4 (1C, CH_3), 41.3 (1C, CH_2), 72.8 (1C, C–OH), 74.5 (1C, C–OH), 126.5, 128.3, 130.7, 137.0 (6C, aromatic carbons). $[\alpha]_{\text{D}}^{20} = -8.9$ ($c = 1.9$, CH_2Cl_2). Enantiomeric excess was determined to 21.3% by analysis of the acetate. Anal. found: C, 73.00; H, 8.80. Calc. for $\text{C}_{11}\text{H}_{16}\text{O}_2$: C, 73.30; H, 8.95%. The racemate was isolated as a colorless solid in quantitative yield; m.p. 63–64 °C.

(3*R*)-2-Methyl-6-phenyl-2-hexene (**8a**) was isolated as a pale yellow oil in 90% yield. ^1H NMR (CDCl_3) 1.14 (s, 3H, CH_3), 1.19 (s, 3H, CH_3), 1.30–1.58 (m, 2H), 1.61–1.77 (m, 1H), 1.86–2.04 (m, 1H), 2.28 (br s, 2H, 2 OH), 2.58–2.75 Hz (m, 2H, CH_2), 3.39 (dd, 10.2 Hz, 2.4 Hz, 1H, CH), 7.15–7.35 (m, 5H, aryl-H). ^{13}C NMR (CDCl_3) 23.2 (1C, CH_3), 26.5 (1C, CH_3), 28.5 (1C, CH_2), 31.2 (1C, CH_2), 35.8 (1C, CH_2), 73.1 (1C, C–OH), 78.3 (1C, C–OH), 125.7, 128.2, 128.3, 142.2 (6C, aromatic carbons). $[\alpha]_{\text{D}}^{20} = 28.3$, ($c = 4.2$, CH_2Cl_2). Enantiomeric excess was determined to 96.7% by analysis of the acetate. Anal.

found: C, 74.66 H, 9.68. Calc. for $\text{C}_{13}\text{H}_{20}\text{O}_2$: C, 74.96; H, 9.68%. The racemate was isolated as a pale yellow oil in quantitative yield.

(2*R*,3*R*)-3-Methyl-6-phenyl-2-hexane diol (**8b**) was isolated as a colorless solid in quantitative yield; m.p. 80–82 °C. ^1H NMR (CDCl_3) 1.09 (s, 3H, CH_3), 1.12 (d, 6.3 Hz, 3H, CH_3), 1.45–1.60 (m, 2H), 1.67–1.80 (m, 2H), 2.08 (br s, 2H, 2 OH), 2.63 (t, 7.5 Hz, 2H, CH_2), 3.64 (q, 6.3 Hz, 1H, CH), 7.15–7.35 (m, 5H, aryl-H). ^{13}C NMR (CDCl_3) 17.5 (1C, CH_3), 20.6 (1C, CH_3), 25.2 (1C, CH_2), 36.4 (1C, CH_2), 38.7 (1C, CH_2), 72.8 (1C, C–OH), 74.9 (1C, C–OH), 125.7, 128.2, 128.3, 142.2 (6C, aromatic carbons). $[\alpha]_{\text{D}}^{20} = 1.3$ ($c = 2.7$, CH_2Cl_2). Enantiomeric excess was determined to 94.2% by analysis of the acetate. Anal. found: C, 74.70 H, 9.67. Calc. for $\text{C}_{13}\text{H}_{20}\text{O}_2$: C, 74.96; H, 9.68%. The racemate was isolated as a colorless solid in 88% yield; m.p. 85–87 °C.

(2*R*,3*S*)-3-Methyl-6-phenyl-2-hexane diol (**8c**) was isolated as a pale yellow oil in 99% yield. ^1H NMR (CDCl_3) 1.13 (d, 6.3 Hz, 3H, CH_3), 1.15 (s, 3H, CH_3), 1.35–1.50 (m, 1H), 1.55–1.88 (m, 3H), 2.05 (br s, 2H, 2 OH), 2.55–2.73 (m, 2H, CH_2), 3.62 (q, 6.3 Hz, 1H, CH), 7.15–7.35 (m, 5H, aryl-H). ^{13}C NMR (CDCl_3) 17.4 (1C, CH_3), 23.5 (1C, CH_3), 25.3 (1C, CH_2), 35.5 (1C, CH_2), 36.5 (1C, CH_2), 74.1 (1C, C–OH), 74.6 (1C, C–OH), 125.7, 128.2, 128.3, 142.3 (6C, aromatic carbons). $[\alpha]_{\text{D}}^{20} = -0.5$ ($c = 0.6$, CH_2Cl_2). Enantiomeric excess was determined to 46.4% by analysis of the acetate. Anal. found: C, 74.72 H, 9.45. Calc. for $\text{C}_{13}\text{H}_{20}\text{O}_2$: C, 74.96; H, 9.68%. The racemate was isolated as a pale yellow oil in quantitative yield.

9. Kinetic measurements in toluene

The competitive stoichiometric dihydroxylations were performed in 2 mL toluene. The two alkenes were added giving a concentration of each of about 1 mg/mL. This allowed direct analysis of the reaction mixture by GC. Two equivalents of (DHQD)₂PHAL with respect to the total amount of alkene were added. *n*-Decane or *n*-tridecane in a concentration of ca 1 mg/mL was used as internal standard. When the difference in reactivity was large (>5) the accuracy in the determination of alkene concentration was improved by using less of the most reactive alkene. After each GC measurement 2 drops of a 0.1 M solution of OsO_4 in toluene were added (about 10 μL). The reaction mixture and the OsO_4 -solution were both kept at 0 °C.

10. Kinetic measurements in *t*-BuOH:H₂O (1:1)

The reaction was performed in 3 mL *t*-BuOH:H₂O (1:1) containing ca 0.03 mmol of each alkene. In addition three equivalents of K_2CO_3 , 10 mol% (DHQD)₂PHAL and 0.5 equivalents of naphthalene (internal standard) relative to the total amount of alkene were added. The resulting suspension was stirred until all solids had dissolved. Then stirring was stopped and the phases were allowed time to separate. 10 μL of the organic layer was withdrawn and

diluted by addition of 20 μL *t*-BuOH. The catalyst was added (5 mol% $\text{K}_2\text{OsO}_2(\text{OH})_4$), and the next sample was withdrawn after 10 min of stirring, again allowing time for phase separation. Each withdrawal of sample from the reaction mixture was followed by the addition of 10 mol% $\text{K}_3\text{Fe}(\text{CN})_6$, and this cycle was repeated 10 times. All the samples were diluted with *t*-BuOH as mentioned above and analyzed by GC immediately or stored in a freezer until analysis could be performed.

Acknowledgements

We thank Jørgen Øgaard Madsen for performing the MS analysis and for assistance in the interpretation of the fragmentation patterns, and DTU for financial support.

References

- [1] S.G. Hentges, K.B. Sharpless, *J. Am. Chem. Soc.* 102 (1980) 4263.
- [2] E.N. Jacobsen, I. Markó, W.S. Mungall, G. Schröder, K.B. Sharpless, *J. Am. Chem. Soc.* 110 (1988) 1968.
- [3] (a) B.B. Lohray, *Tetrahedron: Asymmetry* 3 (1992) 1317;
(b) H.C. Kolb, K.B. Sharpless, in: M. Beller, C. Bolm (Eds.), *Transition Metals for Organic Synthesis*, vol. 2, VCH, Weinheim, 1998, pp. 219–242;
(c) J.S. Svendsen, I. Markó, in: E.N. Jacobsen, A. Pfaltz, H. Yamamoto (Eds.), *Comprehensive Asymmetric Catalysis*, Springer Verlag, Berlin, 1999, pp. 713–790;
(d) R.A. Johnson, K.B. Sharpless, in: I. Ojima (Ed.), *Catalytic Asymmetric Synthesis*, second ed., VCH, New York, 2000, pp. 357–398;
(e) See also: K.A. Jørgensen, in: M. Beller, C. Bolm (Eds.), *Transition Metals for Organic Synthesis*, vol. 2, VCH, Weinheim, 1998, pp. 157–172.
- [4] For selected examples, see: (a) E.M. Carreira, J. Du Bois, *J. Am. Chem. Soc.* 116 (1994) 10825;
(b) Z.-M. Wang, H.C. Kolb, K.B. Sharpless, *J. Org. Chem.* 59 (1994) 5104;
(c) E.J. Corey, A. Guzman-Perez, M.C. Noe, *J. Am. Chem. Soc.* 116 (1994) 12109;
(d) K.C. Nicolaou, C.N.C. Boddy, H. Li, A.E. Koumbis, R. Hughes, S. Natarajan, N.F. Jain, J.M. Ramanjulu, S. Bräse, M.E. Solomon, *Chem. Eur. J.* 5 (1999) 2602;
(e) J.S. Lee, P.L. Fuchs, *Org. Lett.* 5 (2003) 2247.
- [5] (a) K.B. Sharpless, W. Amberg, M. Beller, H. Chen, J. Hartung, Y. Kawanami, D. Lübber, E. Manoury, Y. Ogino, T. Shibata, T. Ukita, *J. Org. Chem.* 56 (1991) 4585;
(b) K.B. Sharpless, W. Amberg, Y.L. Bennani, G.A. Crispino, J. Hartung, K.-S. Jeong, H.-L. Kwong, K. Morikawa, Z.-M. Wang, D. Xu, X.-L. Zhang, *J. Org. Chem.* 57 (1992) 2768.
- [6] H.C. Kolb, P.G. Andersson, K.B. Sharpless, *J. Am. Chem. Soc.* 116 (1994) 1278.
- [7] (a) T. Göbel, K.B. Sharpless, *Angew. Chem., Int. Ed. Engl.* 32 (1993) 1329;
(b) P.-O. Norrby, K.P. Gable, *J. Chem. Soc., Perkin Trans. II* (1996) 171;
(c) E.J. Corey, M.C. Noe, *J. Am. Chem. Soc.* 118 (1996) 319;
(d) D.W. Nelson, K.B. Sharpless, A. Gypser, P.T. Ho, H.C. Kolb, T. Kondo, H.-L. Kwong, D.V. McGrath, A.E. Rubin, P.-O. Norrby, K.P. Gable, *J. Am. Chem. Soc.* 119 (1997) 1840.
- [8] (a) A.K. Rappé, W.A. Goddard III, *J. Am. Chem. Soc.* 104 (1982) 3287;
(b) K.A. Jørgensen, R. Hoffmann, *J. Am. Chem. Soc.* 108 (1986) 1867;
(c) K.A. Jørgensen, *Tetrahedron Lett.* 31 (1990) 6417;
(d) P.-O. Norrby, H.C. Kolb, K.B. Sharpless, *Organometallics* 13 (1994) 344;
(e) A. Veldkamp, G. Frenking, *J. Am. Chem. Soc.* 116 (1994) 4937;
(f) P.-O. Norrby, H. Becker, K.B. Sharpless, *J. Am. Chem. Soc.* 118 (1996) 35;
(g) U. Pidun, C. Boehme, G. Frenking, *Angew. Chem., Int. Ed. Engl.* 35 (1996) 2817;
(h) S. Dapprich, G. Ujaque, F. Maseras, A. Lledós, D.G. Musaev, K. Morukuma, *J. Am. Chem. Soc.* 118 (1996) 11660;
(i) M. Torrent, L. Deng, M. Duran, M. Sola, T. Ziegler, *Organometallics* 16 (1997) 13.
- [9] P.-O. Norrby, H.C. Kolb, K.B. Sharpless, *J. Am. Chem. Soc.* 116 (1994) 8470.
- [10] G. Ujaque, F. Maseras, A. Lledós, *J. Am. Chem. Soc.* 121 (1998) 1317.
- [11] (a) P.-O. Norrby, T. Rasmussen, J. Haller, T. Strassner, K.N. Houk, *J. Am. Chem. Soc.* 121 (1999) 10186;
(b) N. Moitessier, B. Maigret, F. Chrétien, Y. Chapleur, *Eur. J. Org. Chem.* (2000) 995;
(c) N. Moitessier, C. Henry, C. Len, Y. Chapleur, *J. Org. Chem.* 67 (2002) 7275;
(d) N. Moitessier, C. Henry, C. Len, D. Postel, Y. Chapleur, *J. Carbohydr. Chem.* 22 (2003) 25;
(e) G. Drudis-Sole, G. Ujaque, F. Maseras, *Chem. Eur. J.* 11 (2005) 1017.
- [12] (a) E.J. Corey, M.C. Noe, M.J. Grogan, *Tetrahedron Lett.* 37 (1996) 4899;
(b) A.J. Delmonte, J. Haller, K.N. Houk, K.B. Sharpless, D.A. Singleton, T. Strassner, A.A. Thomas, *J. Am. Chem. Soc.* 119 (1997) 9907.
- [13] P. Fristrup, D. Tanner, P.-O. Norrby, *Chirality* 15 (2003) 360.
- [14] (a) P.-O. Norrby, *J. Mol. Struct. (Theochem.)* 506 (2000) 9;
(b) P.-O. Norrby, F. Jensen, *Theor. Chem. Acc.* 109 (2003) 1.
- [15] D.J. Berrisford, C. Bolm, K.B. Sharpless, *Angew. Chem., Int. Ed. Engl.* 34 (1995) 1059.
- [16] (a) E.J. Corey, M.C. Noe, S. Sarshar, *Tetrahedron Lett.* 35 (1994) 2861;
(b) E.J. Corey, M.C. Noe, M.J. Grogan, *Tetrahedron Lett.* 35 (1994) 6427;
(c) E.J. Corey, M.C. Noe, *J. Am. Chem. Soc.* 118 (1996) 11038;
(d) E.J. Corey, J. Zhang, *Org. Lett.* 3 (2001) 3211.
- [17] MacroModel v. 8.0 from Schrodinger Inc.: F. Mohamadi, N.G.J. Richards, W.C. Guida, R. Liskamp, M. Lipton, C. Caulfield, G. Chang, T. Hendrickson, W.C. Still, *J. Comput. Chem.* 11 (1990) 440. For current versions, see: <http://www.schrodinger.com>.
- [18] J.M. Goodman, W.C. Still, *J. Comput. Chem.* 12 (1991) 1110.
- [19] G. Chang, W.C. Guida, W.C. Still, *J. Am. Chem. Soc.* 112 (1990) 1419.
- [20] I. Kolossvary, W.C. Guida, *J. Am. Chem. Soc.* 118 (1996) 5011.
- [21] N. Miyaoura, T. Ishiyama, M. Ishikawa, A. Suzuki, *Tetrahedron Lett.* 52 (1986) 6369.
- [22] N. Miyaoura, T. Ishiyama, H. Sasaki, M. Ishikawa, M. Satoh, A. Suzuki, *J. Am. Chem. Soc.* 111 (1989) 314.
- [23] S.R. Chemler, D. Trauner, S.J. Danishefsky, *Angew. Chem. Int. Ed.* 40 (2001) 4544.
- [24] Y.S. Angelis, M. Orfanopoulos, *J. Org. Chem.* 62 (1997) 6083.